Available online at www.sciencedirect.com
ScienceDirect
Journal of Power Sources 171 (2007) 922–927
JOURNAL OF POWER SOURCES
www.elsevier.com/locate/jpowsour

Short communication

Influence of Mg doping on the performance of $LiNiO_2$ matrix ceramic nanoparticles in high-voltage lithium-ion cells

R. Sathiyamoorthi [a,1], P. Shakkthivel [b,*,2], S. Ramalakshmi [1], Yong-Gun Shul [b,2]

[a] *Department of Industrial Chemistry, Alagappa University, Karaikudi 630003, India*
[b] *Department of Chemical Engineering, Inorganic Materials Lab, Yonsei University, Seodaemun-Ku, Seoul 120-749, Republic of Korea*

Received 23 April 2007; received in revised form 25 May 2007; accepted 6 June 2007
Available online 17 June 2007

Abstract

Nano-crystalline $LiNi_{1-x}Mg_xO_2$ cathode material is synthesized via a novel, simple, solid-state reaction. Thermal analysis studies (TG/DTA) show the formation of crystalline oxides at 600 °C. The influence of Mg addition on the electrochemical behaviour of $LiNiO_2$ is discussed. The morphology, nature, size and the shape of the synthesized materials are characterized by transmission electron microscopy (TEM) and scanning electron microscopy (SEM). $LiNi_{0.8}Mg_{0.2}O_2$ nanoparticles with a size of 40 nm and a uniform distribution and reduced aggregation are observed. Energy dispersive X-ray spectroscopic analysis shows the presence of magnesium in the compounds with an appropriate prepared concentration. The phase and structural characteristics of the $LiNiO_2$ doped and undoped with Mg are revealed by X-ray diffraction spectroscopy (XRD). The addition of Mg does not alter the layered structure of the lithium nickelate. The addition of Mg in the cathode material does not affect the local ion environment, as investigated by FT-IR studies. The electrochemical properties are investigated by cyclic voltammetry (CV) and charge–discharge studies. Stable charge–discharge features have been observed for graphite/$LiNi_{0.8}Mg_{0.2}O_2$ cells cycled in the potential range from 3.0 to 4.5 V and the capacity retention is significantly improved at $x = 0.2$ in $LiNi_{1-x}Mg_xO_2$.

Keywords: Lithium nickelate; Magnesium doping; Cathode material; Lithium-ion cell; Electrochemical studies; Capacity retention

1. Introduction

For the application in lithium-ion batteries, $LiCoO_2$, $LiMn_2O_4$ and $LiNiO_2$ are candidate cathode materials. Among these, $LiNiO_2$ offers a lower cost, higher capacity and better reversibility with voltage range. In addition, it does not cause instability during cycling as it is not prone to reaction with the electrolyte. However, the problem of capacity fading is often encountered because of anisotropic expansion and contraction during the repeated intercalation/de-intercalation process. This behaviour is related to a change in the oxidation state of extra nickel ions which induces local collapse of the structure that hinders not only lithium diffusion in the inter-slab space, but also lithium re-intercalation in the six sites around each extra nickel ion [1]. This behaviour has led to the study of possible alternatives by substituting some of the inter-slab Ni^{2+} ions with cations of nearly the same size with the aim of arresting capacity fading during long-term cycling. The extent of doping and the level of the performance of the doped material depends on the preparation method. Lithium nickelates doped with alkaline-earth elements have been tested as cathode materials in lithium-ion batteries and reported to have very good electrochemical and structural stability [1–11]. In our recent studies, we have demonstrated that $LiCo_{1-x}Mg_xO_2$ offers higher cycleability over a wide potential range [12].

As regards the preparation of Mg-doped lithium nickelate, the present investigation has adopted the solid-state reaction method using urea as the fuel via a nitrate route at an optimum temperature of 600 °C. A series of five lithium-based nickelate compounds with the partial substitution of Mg in the place of Ni in the $LiNiO_2$ matrix at 0, 10, 20, 30 and 50% Mg are prepared by the low-temperature, solid-state reaction method. Earlier research reports have suggested that the percentage of

* Corresponding author. Tel.: +82 2 2123 3554x34; fax: +82 2 312 6401.
E-mail address: apsakthivel@yahoo.com (P. Shakkthivel).
[1] Tel.: +91 4565 228836; fax: +91 4565 230112.
[2] Tel.: +82 2 2123 3554x34; fax: +82 2 312 6401.

0378-7753/$ – see front matter © 2007 Published by Elsevier B.V.
doi:10.1016/j.jpowsour.2007.06.023

Mg content in the LMO matrix is <0.2 in their maximum limits of doping of 0.3 [8,9]. In the present study, however, we have extended the value of x to 0.5 to understand the effect of higher additions of Mg in the original matrix.

2. Experimental

2.1. Synthesis of $LiNi_{1-x}Mg_xO_2$

Analar-grade lithium nitrate, nickel nitrate, magnesium nitrate, ethylene carbonate (EC), dimethyl carbonate (DMC), *N*-methyl-2-pyrolidinone (NMP), polyvinylidene difluoride (PVDF), lithium and $LiBF_4$ were purchased from E-Merck. Graphite powder was obtained from Sisco. All materials were used as-received. $LiNi_{1-x}Mg_xO_2$ materials with different ratios of nickel and magnesium (Mg 0.0–0.5) at an incremental value of 0.1 were synthesized via a low-temperature solid-state reaction. For the preparation of $x = 0.5$ cathode material $LiNO_3 = 0.2012$ g, $Mg(NO_3)_2 = 0.3732$ g and $Ni(NO_3)_2 = 0.4257$ g were weighed accurately and thoroughly mixed to obtain a homogeneous solution with urea as fuel. A 10% excess of $LiNO_3$ was added to avoid the loss of Li as Li_2O. During preparation of the precursor material, glycerol was used as a binder (four drops of glycerol/gram of cathode material was used) that helps the mass of the ingredients to be brought into intimate mixing. A dark-green paste was obtained and heated in an air atmosphere at 150 °C for 2 h. A foam-like, fly ash coloured material was obtained and then crushed. The precursor samples were ignited at 600 °C (pre-determined from thermal studies) for 8 h.

2.2. Structural and surface characterization

The synthesized precursor samples were analyzed for their thermal behaviour by TG/DTA between 20 and 800 °C (Perkin-Elmer Diamond TG/DTA thermal) at a heating rate of 10 °C min^{-1} under an oxygen atmosphere. The purity and structural properties of the synthesized products were investigated with a JEOL (JDX-8030) X-ray diffraction analyzer using Cu Kα radiation. FT-IR spectra were recorded for all the synthesized active cathode materials to confirm the expected moieties in the oxide material; a Perkin Elmer FT-IR spectrophotometer and pressed KBr pellets were employed. To analyze the nature, morphology and distribution of the homogeneous size particles of the synthesized powder, scanning electron microscope (SEM) images were taken with a JEOL (JSM—840A) instrument. The chemical compositions of the synthesized samples were confirmed by energy dispersive X-ray spectroscopic analysis (EDAX) using an X-ray detector attached to a Cambridge S-360 instrument. Transmission electron microscope (TEM) analysis was performed on synthesized nanosized samples of lithium nickel based active cathode materials to determine the crystallization and particle size distribution. A TEM JOEL JEM—2000 EX instrument operated at 200 keV with point-to-point resolution of 2.3 Å was employed.

2.3. Electrochemical characterization

Electrochemical studies of $LiNi_{1-x}Mg_xO_2$ ($x = 0.0$–0.5) were performed by assembling 2016 coin cells with two electrodes. Positive electrodes were prepared from a mixture of 85% synthesized material, 10% acetylene black and 5% polyvinylidene difluoride (PVDF) in *N*-methyl-2-pyrrolidinone (NMP). The resulting mix was coated on to nickel foil, which serves as a current-collector, by applying 2 tonnes cm^{-2} pressure by means of a hydraulic press. The prepared electrodes were stored for 24 h in a vacuum in presence of phosphorous pentoxide (P_2O_5) before use. The coin-type (2016—type) cells were assembled using synthesized $LiNi_{1-x}Mg_xO_2$ electrode cathodes, graphite anode electrodes, Celgard 2600 separator and 1 M $LiBF_4$ electrolyte (50:50 ethylene carbonate (EC)/dimethyl carbonate (DMC)).

In order to assess the topotactical reaction of lithium in the synthesized cathode materials, cyclic voltammetry was used. A two-electrode cell was employed, in which $LiNi_{1-x}Mg_xO_2$ ($x = 0.0$, 0.1, 0.2, 0.3 and 0.5) served as the working electrode and Li metal as the reference and counter electrodes. Cycling was conducted between 3.0 and 4.5 V at a scan rate of 0.1 mV s^{-1} by means of an EG & G Instruments, PAR, Model 6310. Charge–discharge studies were performed at 0.1 mA cm^{-2} in the voltage range of 3.0–4.5 V using a WPG 100 (Pontentiostat/Galvanostat) Won-A-Tech Instrument, South Korea.

3. Results and discussion

3.1. TG/DTA studies

Thermal behaviour of the $LiNi_{1-x}Mg_xO_2$ ($x = 0.1$) precursor sample prepared from lithium nitrate, nickel nitrate and magnesium nitrate with urea as the fuel was studied and the resulting spectra are given in Fig. 1. An initial weight loss of 10% is observed until 150 °C, due to removal of water present in the sample. The consequent two-step loss of 5 and 20 wt.% at 400 and at 550 °C is due to the decomposition of nitrates, i.e., thermal decomposition of urea and glycerol respectively. An exother-

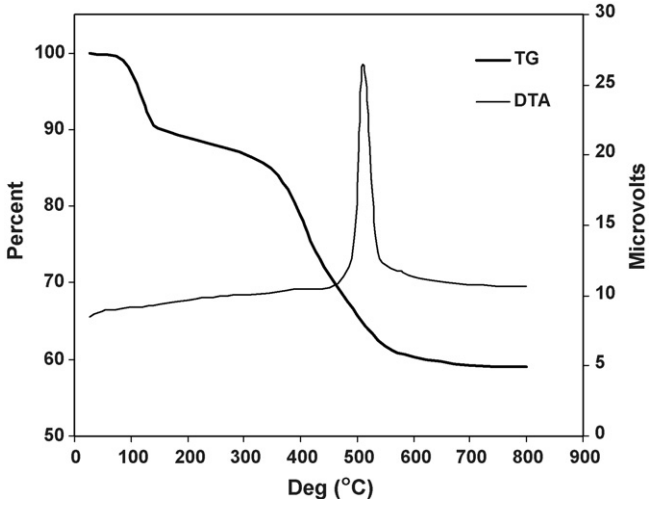

Fig. 1. TG/DTA curves of precursor of $LiNi_{0.9}Mg_{0.1}O_2$.

mic peak at 600 °C is observed, which indicates the formation of crystalline solid material. No further weight loss is observed beyond 600 °C and this can be interpreted as clear evidence of compound formation. Hence, for the cathode material synthesis, the solid-state reaction method at 600 °C was followed.

3.2. XRD studies

Powder X-ray diffraction patterns of undoped $LiNiO_2$ and Mg-doped $LiNiO_2$ synthesized at 600 °C with Mg incorporation of 10, 20, 30, and 50% are presented in Fig. 2. The XRD pattern of the $LiNi_{1-x}Mg_xO_2$ sample shows one well-defined peak of high intensity at $2\theta = 19°$ and two other less intense peaks at 36° and 44°. The data for intensity versus diffraction angle peak indicates that the compound crystallizes as a rhombohedral system (space group *R*3*m*) [13,14]. There are no additional peaks, which indicates the absence of other phases. The lattice constants, computed from XRD data, vary as a function of Mg^{2+}, i.e., with the progressive addition of Mg^{2+}, a slight decrease in the lattice value *a* and an increase in the *c* values are observed and the unit cell volume decreases by 2%. The results are presented in Table 1. A distinct splitting of (0 0 6) (1 0 2) and (1 0 8) (1 1 0) doublets is observed for $LiNiO_2$ at a low concentration of Mg doping. When the Mg concentration is increased, however, the splitting of (0 0 6) (1 0 2) and (1 0 8) (1 1 0) doublets tends to merge and the remaining peaks are slightly broadened. This is an indication of a reduced crystallite size coupled with microscopic strain in the crystal lattice that could be due to a certain degree of mismatch in the Mg^{2+} (0.66 Å) and Ni^{3+} (0.56 Å) ionic sizes. These observations and the values of $I_{(0\,0\,3)}/I_{(1\,0\,4)} \approx 1.22$ have been considered as a qualitative measure of the improved cathodic activity of the synthesized compounds [15]. The maximum $I_{(0\,0\,3)}/I_{(1\,0\,4)}$ value of 1.343 is observed at $x = 0.2$. This indicates an enhanced stabilization of Ni^{3+} in the 2D-layered structure on Mg substitution at $x = 0.2$ [15]. For every assigned (*h k l*) indices, lattice parameters are rightly assigned to compute constant values of the lattice parameters as least-squares mean values of *a* and *c* in case of hcp or hexagonal and tetragonal crystal systems [16–19]. It is reported for minimum Mg-substituted lithium nickelates ($y \leq 0.02$), lithium deficiency is required for the presence of all Mg^{2+} ions in the inter-slab space. With the addition of $Mg \leq 0.2$ in the $LiNiO_2$, a large amount of Mg^{2+} ions are located in the lithium site [1]. The presence of magnesium ions in the lithium site prevents any local collapse of the inter-slab space during the de-intercalation process.

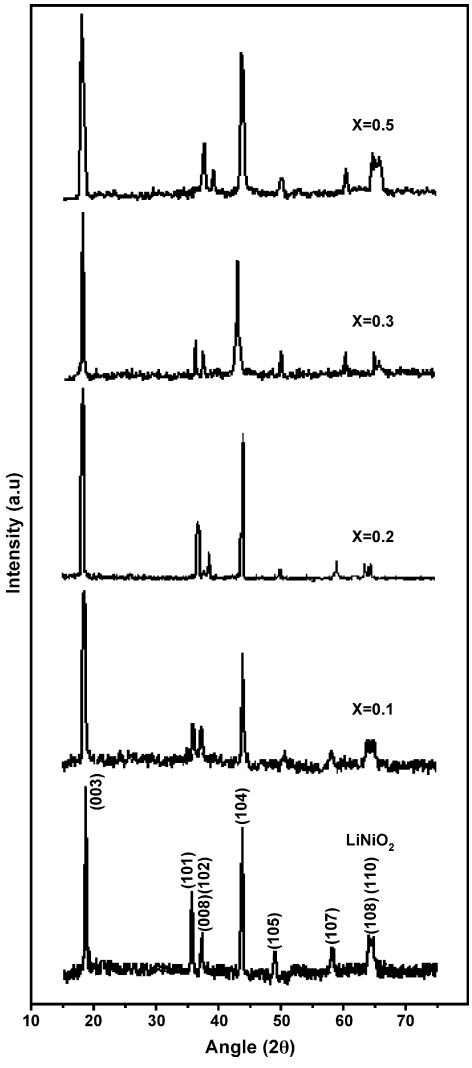

Fig. 2. XRD patterns of $LiNi_{1-x}Mg_xO_2$ ($x = 0.0$, 0.1, 0.2, 0.3 and 0.5).

Table 1
XRD lattice constants *a*, *c*, *c*/*a* ratio, unit-cell volume and $I_{(0\,0\,3)}/I_{(1\,0\,4)}$ for Mg-doped $LiNiO_2$ and undoped $LiNiO_2$

Sample	*a* (Å)	*c* (Å)	*c*/*a*	Unit cell volume (Å)^3	$I_{(0\,0\,3)}/I_{(1\,0\,4)}$
$LiNiO_2$	2.8775	14.2144	4.9398	101.81	1.222
$LiNi_{0.9}Mg_{0.1}O_2$	2.8763	14.2162	4.9425	101.73	1.235
$LiNi_{0.8}Mg_{0.2}O_2$	2.8760	14.2169	4.9467	101.71	1.343
$LiNi_{0.7}Mg_{0.3}O_2$	2.8758	14.2175	4.9473	101.70	1.252
$LiNi_{0.5}Mg_{0.5}O_2$	2.8753	14.2181	4.9484	101.58	1.196

3.3. FT-IR studies

In addition to the XRD experimental results, further evidence for the formation of $LiNi_{1-x}Mg_xO_2$ materials has been obtained from FT-IR experimental data. The purpose of this study is to investigate the local environment cations in a cubic-close packed oxygen array of the $LiNi_{1-x}Mg_xO_2$ lattice. According to factor group analysis, the infrared spectra of $LiMO_2$ (M = Metals) compounds with *R*3*m* space group yield four infrared-active modes [20,21]. Fig. 3 depicts the mode of vibrations for $LiNi_{1-x}Mg_xO_2$ in the 400–700 cm^{-1} region that are largely associated with the vibrations of NiO_6 and LiO_6 octahedral units [22,23]. The peaks at 627 and 687 cm^{-1} are the bending vibrations modes of NiO_6, i.e., ν[(Ni–O–Li)], the weak band at around 432 cm^{-1} is assigned to the asymmetric stretching of Li–O in LiO_6 environments [22,23].

In addition to these bands, a band at about 271 cm^{-1} in the far-IR region is expected but that region is not covered in the present study [24]. With respect to the waves at low frequency, the isotopic replacement in $LiNiO_2$ has proved that the band

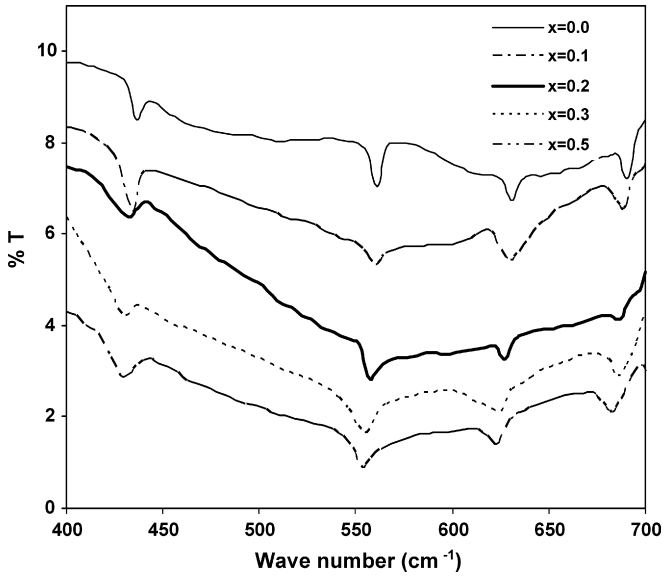

Fig. 3. FT-IR spectra of $LiNi_{1-x}Mg_xO_2$.

between 200 and 300 cm^{-1} is associated with vibration of a relatively isolated LiO_6 octahedron [25]. The shape of the IR absorption spectra (Fig. 3) for the Mg-doped cathode materials remains the same as that of $LiNiO_2$, apart from a slight overall shift in the peaks towards lower frequency values which shows that the local environment of lithium ions surrounded by oxygen anions is not affected and there is little increase in NiO_2 layer covalency [6]. At higher magnesium substitution, the broadening of the peaks can be interpreted as NiO_6 distortion due to magnesium induction in NiO_2 layers.

3.4. TEM studies

The TEM photographs for undoped and Mg-doped $LiNiO_2$ ($x = 0.2$) synthesized at 600 °C are presented in Fig. 4a and b, respectively. In the case of undoped $LiNiO_2$, the cluster formation is ≈60 nm. This is little larger when compared with the Mg-doped material (≈40 nm) and the particle size is smaller. The interlayer distance may be higher in the undoped $LiNiO_2$ than that of the doped one, due to the larger size of the particles. The surface area of the electrode material is an important parameter that determines the energy and power density of a particular battery system. In the present study, the surface area is expected to be higher for the Mg-doped cathode material because of its smaller particle size.

3.5. SEM with EDAX studies

Scanning electron micrographs were taken for Mg-doped ($x = 0.2$) and undoped synthesized lithium nickelates, as shown in Fig. 5a and b, respectively. Lithium insertion and de-insertion of the electrode mainly depend on the morphological structure of the material. Hence, morphological studies are highly essential. The micrographs show that the particles of the Mg-doped cathode material are of nanometer size; the average diameter of the particles of the cathode material is about 40 nm. Among the synthesized cathode materials for lithium battery applications, $x = 0.2$ magnesium-doped lithium nickelate shows a well-reduced particle size with less particle aggregation and a uniform particle distribution. It can be expected that the intercalation/de-intercalation will be much easier in $LiNi_{0.8}Mg_{0.2}O_2$ because of the reduced path length for lithium migration during the charging–discharging process. As the consequence, higher capacity retention, longer cycle-life and greater power density are to be anticipated with $LiNi_{0.8}Mg_{0.2}O_2$.

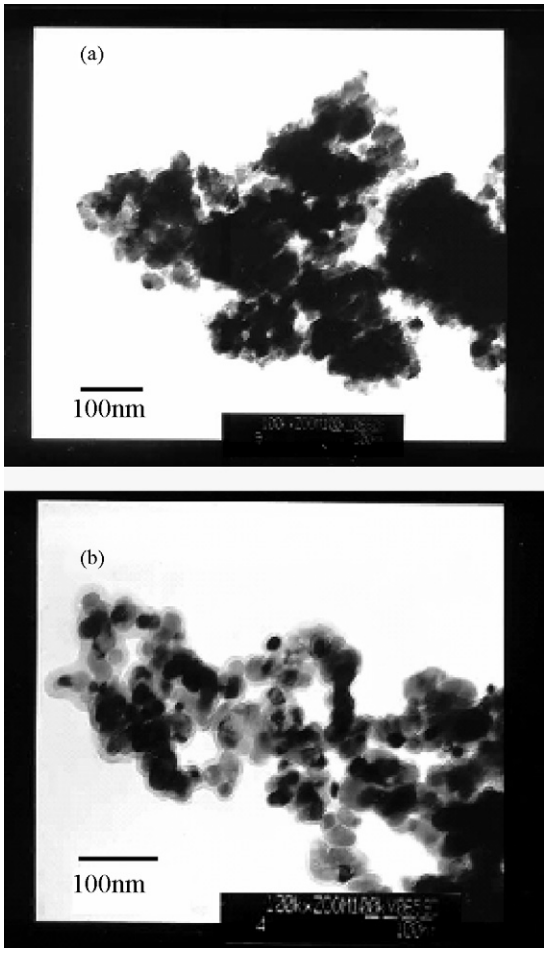

Fig. 4. TEM photograph of (a) $LiNiO_2$ and (b) $LiNi_{0.8}Mg_{0.2}O_2$.

To determine the composition of synthesized Mg-doped $LiNiO_2$ nanoparticle materials, EDAX studies were carried out and the data are presented in Table 2. The composition parameters show the presence of Mg in an appropriate percentage along with Ni.

Table 2
EDAX composition analysis of $LiNi_{1-x}Mg_xO_2$ ($x = 0.1$, 0.2, 0.3 and 0.5)

x in $Li_{1-x}Mg_xO_2$	Nickel ratio (%)	Magnesium ratio (%)
0.1	90.09	9.91
0.2	79.98	20.02
0.3	69.22	30.78
0.5	51.94	48.06

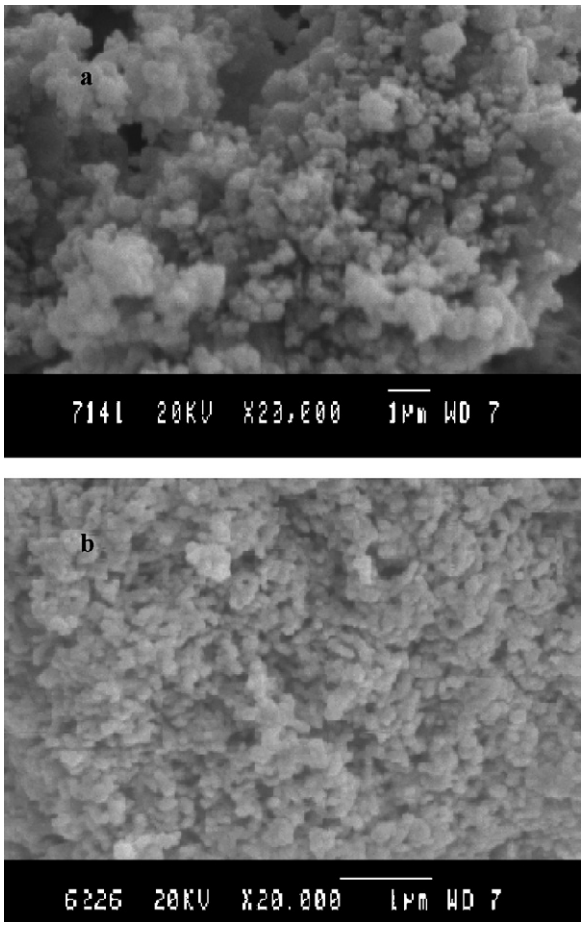

Fig. 5. SEM photograph of (a) $LiNiO_2$ and (b) $LiNi_{0.8}Mg_{0.2}O_2$.

3.6. Cyclic voltammograms

The redox properties of the synthesized cathode materials for lithium-ion batteries were examined by means of cyclic voltammetry experiment; the results are given in Fig. 6. Cyclic voltammograms for $LiNi_{1-x}Mg_xO_2$ ($x = 0.0$, 0.1, 0.2, 0.3 and 0.5) cells show the existence of a reversible structure property by their redox activity. From the *I–V* curves, the intercalation and de-intercalation process of Li^+ over the potential range of 3.0–4.5 V are seen. The sample prepared at $x = 0.2$ exhibits the minimum peak potential separation; $\Delta E_p = 120$, 98, 79, 151 and 192 mV for $x = 0.0$, 0.1, 0.2, 0.3 and 0.5 Mg, respectively.

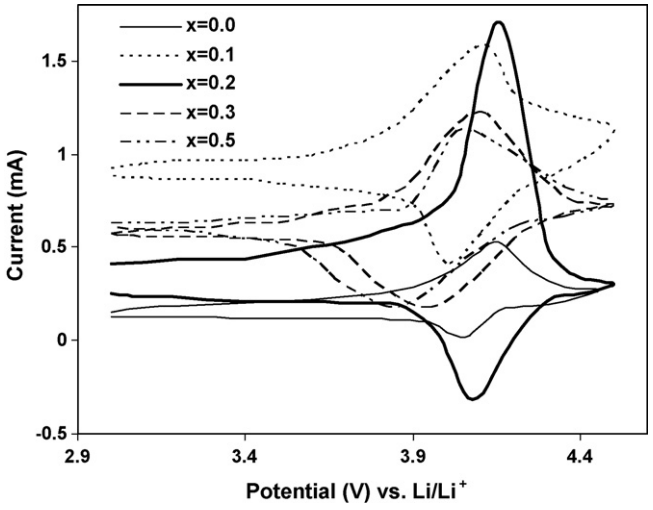

Fig. 6. Cyclic voltammograms of Mg-doped $LiNiO_2$ and undoped $LiNiO_2$ cathode materials at scan rate of 0.1 mV s^{-1}.

3.7. Charge–discharge studies

$LiNi_{1-x}Mg_xO_2$ cathode electrodes were examined for their charge/discharge properties by testing within a potential window of 3.0–4.5 V at a constant current density of 0.1 mA cm^{-2} using the assembled button cells. The voltage versus capacity profiles of all doped and undoped $LiNiO_2$ materials in the first charge/discharge curves are presented in Fig. 7. During the first cycle, the cell efficiency was 87.3% for $x = 0.0$. The first coulombic cell efficiencies increase with gradual substitution of Mg with Ni up to certain limit ($x = 0.2$), beyond that, there is a declining trend at higher addition of Mg with $x = 0.3$ and $x = 0.5$, which indicates that the doping instead of being beneficial appears to be detrimental at such high doping levels. It is clear from the results that the irreversible capacity for the first cycle is least for $x = 0.2$ and maximum for $x = 0.5$ compared with undoped cell. The reversible capacity at the end of 25th cycle is the maximum for $x = 0.2$ and minimum for $x = 0.5$ (Fig. 8). The findings are summarized in Table 3. The $LiNi_{0.8}Mg_{0.2}O_2$ material exhibits a higher value of 97.6% discharge capacity retention at the end of 25th cycle. Thus, the capacity fading is very much arrested with a doping of Mg of $x = 0.2$. In the Li_xNiO_2 system, the dramatic deterioration of electrochemical performance is strongly related to the change in the oxidation state of the extra nickel ions, which induces local collapse of the structure and hinders not only lithium diffusion in the inter-slab space but also lithium reintercalation in the six sites around each extra nickel ion [1,26,27]. In the $Li_xNi_{1-y}Mg_yO_2$ system, the magnesium ions, with a size close to that of lithium, remain in the divalent state during cell charge. Therefore, their presence in the inter-slab space does not strongly affect lithium re-intercalation because no shrinkage of the structure occurs upon cycling. This result explains

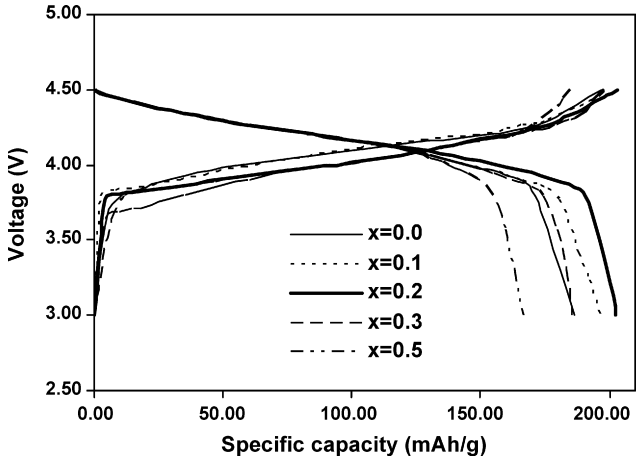

Fig. 7. First charge–discharge curves of $LiNiO_2$ and $LiNi_{1-x}Mg_xO_2$ ($x = 0.0$, 0.1, 0.2, 0.3 and 0.5).

Table 3
Cathode charge–discharge and irreversible capacities of the compounds, $LiNi_{1-x}Mg_xO_2$

Properties	$x=0.0$	$x=0.1$	$x=0.2$	$x=0.3$	$x=0.5$
First charge capacity (mAh g^{-1})	197	199	203	198	185
First discharge capacity (mAh g^{-1})	172	180	190	174	157
Irreversible capacity for the first cycle (mAh g^{-1})	25	19	13	24	28
Reversible capacity in 25th cycle (mAh g^{-1})	157	175.2	185.4	167.5	149.4
Discharge capacity retention in 25th cycle (%)	91.3	97.3	97.6	96	95.2

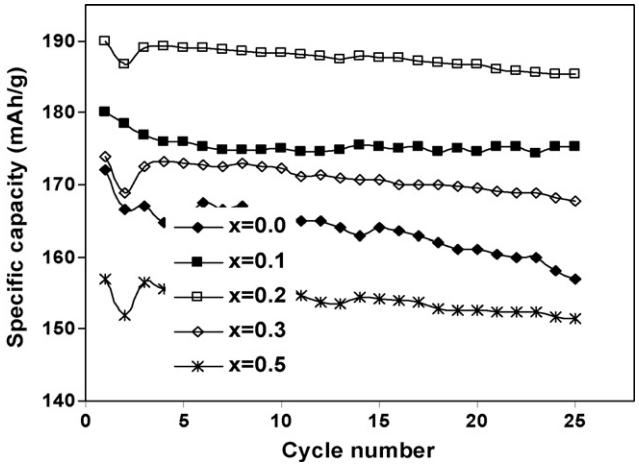

Fig. 8. Plots of specific capacity vs. cycle number of $LiNiO_2$ and $LiNi_{1-x}Mg_xO_2$ ($x=0.0$, 0.1, 0.2, 0.3 and 0.5).

how the magnesium-substituted phases have good cycling properties with enhanced capacity. The presence of an optimum concentration of magnesium ions in the lithium site prevents any local collapse of the inter-slab space during the de-intercalation process.

At a higher dosage of Mg^{2+} ions in the cathode material, the Ni^{2+} preferentially occupies in the inter-slab spacing during the electrochemical process, which causes the low capacity delivery. On the other hand, the presence of Mg^{2+} ions in the lithium sites at the optimum concentration significantly reduces the usual changes observed in the cell parameters and accounts for good capacity retention.

4. Conclusions

Mg-substituted $LiNiO_2$ nano-crystalline materials have been synthesized with stoichiometric compositions of $LiNi_{1-x}Mg_xO_2$ ($x=0.0$, 0.1, 0.2, 0.3 and 0.5) by means of a low-temperature (600 °C) solid-state reaction. Enhanced reversibility of the Li intercalation/de-intercalation reaction is obtained with a cathode prepared at $x=0.2$. This assists the intercalation processes by stabilizing the host matrix without collapse. Charge–discharge studies carried out at 0.1 mA cm^{-2} for all the compounds ($0.0<x<0.3$), reveal better capacity retention and cycleability compared with un-substituted $LiNiO_2$. Consequently, $LiNi_{0.8}Mg_{0.2}O_2$ is a promising cathode material for high performance Li-ion cells.

References

[1] C. Pouillerie, L. Croguennec, Ph. Biensan, P. Willmann, C. Delmas, J. Electrochem. Soc. 147 (6) (2000) 2061.
[2] P. Kalyani, PhD thesis, Alagappa University, July 2003.
[3] C.C. Chang, J.Y. Kim, P.N. Kumta, J. Electrochem. Soc. 147 (5) (2000) 1722.
[4] P.N. Kumta, C.C. Chang, M.A. Sriram, US Patent 6,017,654 (2000).
[5] M. Hasegawa, Y. Bito, S. Ito, T. Murata, Y. Toyoguchi, US Patent 5,631,105 (1997).
[6] C. Julien, G.A. Nazri, A. Rougier, Solid State Ionics 135 (2000) 121.
[7] K. Takanishi, Y. Matsuda, J. Tsukamoto, US Patent 5,679,481 (1997).
[8] C. Pouillerie, L. Croguennee, C. Delmas, Solid State Ionics 132 (2000) 15.
[9] C. Delmas, M. Menetrier, L. Croguennee, I. Saadoune, A. Rougier, C. Pouillerie, G. Prado, M. Grune, L. Fournes, Electrochim. Acta 45 (1999) 243.
[10] R. Sathiyamoorthi, T. Vasudevan, Electrochem. Commun. 9 (2007) 416.
[11] R. Sathiyamoorthi, T. Vasudevan, Mater. Res. Bull., in press.
[12] R. Sathiyamoorthi, P. Shakkthivel, R. Gangadharan, T. Vasudevan, Ionics 13 (1) (2007) 25.
[13] C.H. Lu, L.W. Cheng, J. Mater. Chem. 10 (2000) 1403.
[14] M. Mohan Rao, C. Liebenow, M. Jayalakshmi, H. Wulff, U. Guth, F. Scholz, J. Solid State Electrochem. 5 (2001) 348.
[15] J. Morales, C. Perez-Vicente, J.L. Tirado, Mater. Res. Bull. 25 (1990) 623.
[16] L.V. Azaroff, M.J. Buerger, The Powder Method, McGraw-Hill, 1976.
[17] H.P. Klug, L.E. Alexander, X-ray Diffraction Procedure, John Wiley, 1967.
[18] C. Barrett, T.B. Massalski, Structure of Metals, 3rd ed., McGraw-Hill, Eurasia, 1968.
[19] B.D. Cullity, Elements of X-ray Diffraction, 2nd ed., Addison-Wesley, 1978.
[20] R.K. Moore, W.B. White, J. Am. Ceram. Soc. 53 (1970) 679.
[21] W.W. Huang, R. Frech, Solid State Ionics 86–88 (1996) 395.
[22] S.R.S. Prabakaran, M.S. Michael, S. Radhakrishnan, C. Julien, J. Mater. Chem. 7 (1997) 1791.
[23] J. Preudhomme, P. Tarte, J. Spectrochim. Acta A 28 (1972) 69.
[24] E. Zhecheva, R. Stoyanova, Solid State Ionics 66 (1993) 143.
[25] P. Tarte, J. Preudhomme, J. Spectrochim. Acta A 26 (1970) 747.
[26] J.P. Peres, C. Delmas, A. Rougier, M. Broussely, F. Perton, Ph. Biensan, P. Willmann, J. Phys. Chem. Solids 57 (1996) 1057.
[27] C. Delmas, J.P. Peres, A. Rougier, A. Demourgues, F. Weill, A. Chadwick, M. Broussely, F. Perton, Ph. Biensan, P. Willmann, J. Power Sources 68 (1997) 120.